

1
2
3
4
5
6
7
8
9
10
11
12
13
14
15
16
17
18
19
20
21
22
23
24
25
26
27
28

Evaluation of Long-Term Cloud-Resolving Model Simulations Using
Satellite Radiance Observations and Multi-Frequency Satellite Simulators

Toshihisa Matsui^{1,2}, Xiping Zeng^{1,2}, Wei-Kuo Tao¹, Hirohiko Masunaga³, William S.
Olson^{1,4}, and Stephen Lang^{1,5}

¹ Laboratory for Atmospheres, NASA Goddard Space Flight Center, Greenbelt,
Maryland, USA

² Goddard Earth Science and Technology Center, University of Maryland Baltimore
County, Baltimore, Maryland, USA

³Hydrospheric Atmospheric Research Center Nagoya University, Nagoya, Japan

⁴Joint Center for Earth Systems Technology, University of Maryland Baltimore County,
Baltimore, Maryland, USA

⁵ Science Systems and Applications Inc, Lanham, Maryland, USA

Submitted to Journal of Atmospheric and Oceanic Technology
on May 2 2008

Corresponding Author:

Toshihisa Matsui
Code 613.1, NASA Goddard Space Flight Center
Greenbelt, MD 20771
Tell: 301-614-5658
Email: Toshihisa_Matsui-1@nasa.gov

1 **Abstract.**

2 This paper proposes a methodology known as the Tropical Rainfall Measuring
3 Mission (TRMM) Triple-Sensor Three-step Evaluation Framework (T3EF) for the
4 systematic evaluation of precipitating cloud types and microphysics in a cloud-resolving
5 model (CRM). T3EF utilizes multi-frequency satellite simulators and novel statistics of
6 multi-frequency radiance and backscattering signals observed from the TRMM satellite.
7 Specifically, T3EF compares CRM and satellite observations in the form of combined
8 probability distributions of precipitation radar (PR) reflectivity, polarization-corrected
9 microwave brightness temperature (Tb), and infrared Tb to evaluate the candidate CRM.

10 T3EF is used to evaluate the Goddard Cumulus Ensemble (GCE) model for cases
11 involving the South China Sea Monsoon Experiment (SCSMEX) and Kwajalein
12 Experiment (KWAJEX). This evaluation reveals that the GCE properly captures the
13 satellite-measured frequencies of different precipitating cloud types in the SCSMEX case
14 but underestimates the frequencies of deep convective and deep stratiform types in the
15 KWAJEX case. Moreover, the GCE tends to simulate excessively large and abundant
16 frozen condensates in deep convective clouds as inferred from the overestimated GCE-
17 simulated radar reflectivities and microwave Tb depressions. Unveiling the detailed
18 errors in the GCE's performance provides the best direction for model improvements.

19

20

21

22

23

1 **1. Introduction**

2 Cloud-resolving models (CRMs) explicitly resolve convective clouds and cloud
3 systems on fine spatial and temporal scales for relatively short-time periods. A one-
4 moment-bulk microphysics scheme predicts the evolution of liquid and ice condensates
5 and their associated latent heating and evaporative cooling in contrast to the implicit
6 prediction in single-column schemes (Tao et al. 2003). With significant improvements in
7 computational power over the last decade, CRM simulations can now be conducted for
8 longer time periods in a 3D model configuration to obtain a better understanding of cloud
9 and precipitation ensembles and radiative-convective equilibrium (Zeng et al. 2007; Zhou
10 et al. 2007; Blossey et al. 2007; and many others). While they explicitly simulate cloud
11 dynamics and microphysics evolution, CRMs are still subject to many uncertainties in
12 cloud microphysical processes due to a lack of practical evaluation frameworks that can
13 contrast CRM simulations with routine, extensive observations such as satellite
14 measurements. Lang et al. (2007) recently initiated a more systematic approach to
15 improving the microphysics in the Goddard Cumulus Ensemble model (GCE) based
16 mainly on probability distributions from ground-based radar observations and limited
17 satellite observations, but the two simulations used in the study were short-term and from
18 a single location.

19 The Tropical Rainfall Measuring Mission (TRMM) satellite has operated
20 continuously for over a decade, providing numerous, valuable observations of
21 precipitating tropical cloud systems from its sensors: the Visible/Infrared Scanner
22 (VIRS), TRMM Microwave Imager (TMI), and Precipitation Radar (PR, Kummerow et
23 al. 1998). The retrieved rainfall rates and hydrometeor products are useful datasets for

1 model evaluation (e.g., Zhou et al. 2007). However, TRMM-derived physical products
2 could contain their own biases due to uncertainties in the particle size spectra, particularly
3 at the freezing level, in the retrieval algorithms (Kummerow et al. 2006). Therefore, it is
4 often difficult to make a detailed evaluation of CRMs using TRMM-derived physical
5 products due to differences in their estimation methods and microphysics assumptions.
6 Thus, in order to evaluate CRMs more precisely against satellite observations, it is
7 preferable to estimate satellite-consistent radiances from the model-generated
8 microphysical distributions using radiative transfer calculations (i.e., satellite simulators,
9 Chaboureau et al. 2002; Chevallier and Bauer 2003; Masunaga et al. 2008), since direct
10 satellite measurements (radiances) have much less uncertainty than retrieved physical
11 parameters.

12 This paper introduces a practical CRM-evaluation framework using multi-
13 frequency satellite simulators and fine-resolution radiance measurements from the
14 TRMM satellite. The evaluation framework consists of i) a CRM coupled with multi-
15 frequency satellite simulators and ii) a three-step statistical evaluation of brightness
16 temperatures (Tbs) and radar reflectivities from the CRM simulations and TRMM
17 observations. The approach is applied to long-term simulations from the GCE for two
18 cases: the South China Sea Monsoon Experiment (SCSMEX) and the Kwajalein
19 Experiment (KWAJEX). These two cases are based on well-established field campaigns
20 and have already been used previously for long-term CRM simulations to study tropical
21 cloud and precipitation processes (Zeng et al. 2007; Zhou et al. 2007; Blossey et al.
22 2007). Those studies demonstrated that CRMs driven by the large-scale forcing could

1 simulate the general features of the observed cloud processes but with essentially similar
2 biases.

3 Zeng et al. (2007) found that the GCE tended to overestimate surface precipitation
4 throughout the simulation periods for both SCSMEX and KWAJEX, and, as a result,
5 column-integrated water vapor was largely underestimated compared to observations.
6 They also found more convective cores with stronger updrafts in the 3D model
7 configuration than in the 2D; therefore, regardless of the chosen microphysical
8 parameterization, simulated precipitating cloud systems can be quite sensitive to
9 differences in the dimensionality of the model. Zhou et al. (2007) found that GCE
10 simulations for the SCSMEX case tended to produce a slightly larger convective to
11 stratiform rain ratio than was estimated from the PR and TMI due to having less anvil
12 (stratiform) cloud. They also found that underestimated high cloud fractions lead to an
13 overestimation of outgoing longwave radiation in comparison with that estimated from
14 Clouds and the Earth's Radiant Energy System (CERES) sensors. Although using a
15 different CRM and different observational data, Blossey et al. (2007) also found that their
16 CRM also tended to underestimate high-cloud fraction, leading to an overestimate of the
17 outgoing longwave radiation and an underestimate of the top-of-the-atmosphere (TOA)
18 albedo during less rainy periods. These studies evaluated the CRM physical parameters
19 as domain-averaged values.

20 In contrast to the previous studies, this paper focuses on a satellite radiance-based
21 systematic evaluation of long-term CRM simulations by assessing the frequency of
22 occurrence of different precipitation types as well as the microphysics of each
23 precipitation type using multi-frequency satellite simulators. The paper is organized as

1 follows. Section 2.1 details the configuration and setup of the long-term CRM
2 simulations for the KWAJEX and SCSMEX cases. Section 2.2 describes the TRMM
3 multi-sensor observations and the combinations used for evaluation. Section 2.3
4 describes the multi-sensor satellite simulators. Section 3 introduces a new satellite-based
5 CRM evaluation framework. The framework is then used to evaluate the long-term CRM
6 simulations in section 4. Section 5 discusses and summarizes issues related to the CRM
7 simulations raised by the evaluation.

8

9

10 **2. Numerical Experiments and Satellite Measurements**

11 **2.1 Cloud-Resolving Model Simulations**

12 In this study, long-term CRM simulations are performed using the GCE model
13 (Tao 2003) for environments observed during the SCSMEX and KWAJEX field
14 campaigns. The simulations are driven by surface turbulent fluxes, large-scale advective
15 forcing for temperature and humidity, and horizontal wind tendencies derived from
16 objective analysis, which statistically combines a variety of field measurements (Zhang et
17 al. 2001). For a given high-quality long-term meteorological forcing, the GCE with
18 imposed forcing provides a way to evaluate model configurations and physical processes
19 (including the microphysics and cloud properties), if the simulated fields can be validated
20 using independent observations. Two microphysics schemes are used in this study. One
21 is the default Goddard microphysics (denoted as GM03) with three-ice species (Tao
22 2003), and the other is a newly-implemented microphysics scheme (denoted as GM07,
23 Zeng et al. 2007; Lang et al. 2007). GM07 includes ice-nuclei concentrations for the

1 Bergeron process (Zeng et al. 2007) and lowered collection efficiencies to reduce
2 excessive amounts of graupel (Lang et al. 2007).

3 The grid configurations, dynamic core, and other physical parameterizations are
4 identical except for the microphysics schemes (i.e., GM03 and GM07). The grid domain
5 consists of $256 \times 256 \times 41$ grid points in a Cartesian coordinate with a horizontal grid
6 spacing of 1 km. The simulation domain is centered at 9°N and 167°E for the KWAJEX
7 case and at 21°N and 116°E for the SCSMEX case. The time step is 6 seconds, and the
8 simulations periods are from July 24 to September 14, 1999 for KWAJEX and from May
9 6 to June 14, 1998 for SCSMEX (Zeng et al. 2007).

10 Zeng et al. (2007) examined the sensitivity of simulated precipitation condensate
11 to model dimensionality (i.e., 2D versus 3D grids) and microphysics (i.e., GM03 and
12 GM07). Because precise and extensive measurements of water contents and drop-size
13 distributions (DSDs) of precipitation particles are limited even within a well-designed
14 field campaign, in the present study, these uncertain microphysical parameters are best
15 evaluated through their impact on simulated multi-frequency radiance and backscattering
16 signals in contrast to satellite observations (Chaboureau et al. 2002; Chevallier and Bauer
17 2003; Masunaga et al. 2008).

18

19

20 **2.2 TRMM Measurements**

21 In this study, TRMM PR 13.8-GHz attenuation-corrected reflectivity from the
22 TRMM 2A25 product, VIRS 12- μm infrared brightness temperature (T_{bIR}) from TRMM
23 1B01, and TMI 85.5-GHz dual-polarization microwave brightness temperature (T_{b85})

1 from TRMM 1B11 (Kummerow et al. 1998) are used to evaluate the GCE simulations.
 2 PR reflectivity is sensitive to precipitating liquid and frozen condensates. VIRS Tb_{IR}
 3 represents the cloud-top temperature above optically thick clouds. TMI Tb_{85} depression
 4 (i.e., scattering) is correlated with the amount of precipitation-sized ice particles (Liu and
 5 Curry 1996). Observations from these three sensors were collected over the KWAJEX
 6 and SCSMEX sites during the GCE simulation periods. Significant PR reflectivity
 7 (above 17 dBZ) is also used to identify the radar echo-top height (H_{ET}). Because the TMI
 8 sampled mixed land-ocean areas over the KWAJEX and SCSMEX sites, a polarization-
 9 corrected brightness temperature ($PCTb_{85}$) is computed (Kidd 1998) in order to
 10 compensate for the inhomogeneity of surface emissivity via

$$11 \quad PCT_{85} = Tb_{85V} + a(Tb_{85V} + Tb_{85H}),$$

12 where Tb_{85V} and Tb_{85H} are the Tb from the vertical and horizontal polarization channels at
 13 85 GHz, respectively, and $a=0.8$, which ensures that the inhomogeneity in surface
 14 emission is visually masked out over the two sites. VIRS Tb_{IR} and TMI $PCTb_{85}$ are
 15 collocated on the PR instantaneous field of view (IFOV). The PR and high-frequency
 16 TMI measurements have a fine IFOV of ~ 5 km, close to the horizontal resolution of
 17 typical CRMs (i.e., $dx=dy=1$ km in this study; thus a minimum resolvable dynamical-
 18 spatial scale for the GCE simulations should be ~ 5 km). VIRS Tb_{IR} measurements are
 19 convolved within the PR IFOV (i.e., 4.3 km at the surface) via a Gaussian beam pattern
 20 due to the smaller IFOV (i.e., 2.2 km at the surface) of the VIRS measurements
 21 (Masunaga and Kummerow 2005).

22

23 **2.3 Satellite Simulators**

1 The Goddard Satellite Data Simulation Unit (SDSU) is an end-to-end satellite
2 simulator being built upon the original version developed at HyARC, Nagoya University
3 (available from <http://precip.hyarc.nagoya-u.ac.jp/sdsu/sdsu-main.html>). The Goddard
4 SDSU simulates satellite-consistent radiances or backscattering from vertical profiles of
5 model-simulated atmospheric variables and condensates obtained from the Goddard
6 Multi-Scale Modeling System with unified physics (Tao et al. 2008). At present, the
7 framework includes passive microwave, radar, visible-infrared, lidar, broadband
8 shortwave and longwave, and ISCCP-like simulators.

9 In this study, GCE-simulated atmospheric and condensate profiles are used to
10 simulate TRMM PR-consistent reflectivity profiles via a radar simulator (Masunaga and
11 Kummerow 2005), VIRS-consistent Tb_{IR} through a spectrum infrared simulator (discrete
12 ordinate radiative transfer, Nakajima and Tanaka 1986; Stamnes et al. 1988), and TMI-
13 consistent Tb_{85} through a passive microwave simulator (delta-Eddington two-stream
14 radiative transfer with slant path view, Kummerow 1993; Olson and Kummerow 1996).
15 All of the simulators are currently 1D and do not include 3D scattering effects. Within
16 the simulators, the optical properties for condensates are derived via Mie theory
17 (spherical assumption), while the DSD parameters for precipitation particles are specified
18 in accordance with the GCE model (i.e., exponential size distributions with prescribed
19 exponent-intercept parameters and particle densities). The simulated Tbs and radar
20 reflectivities are then convolved within the IFOV corresponding to each TRMM sensor
21 through a Gaussian beam pattern (Masunaga and Kummerow 2005) and sampled only at
22 the actual TRMM orbiting time over the respective KWAJEX or SCSMEX sites. It

1 should be noted that CRM-simulated non-precipitating cloud systems are not evaluated in
2 this framework.

3

4 **3. TRMM Triple-sensor Three-step Evaluation Framework (T3EF)**

5 Due to the inability of CRMs to accurately predict the location of precipitating
6 cloud systems relative to the satellite observations, ensemble statistics of Tbs and radar
7 reflectivities from the satellite observations and GCE simulations are compared. As a
8 result, it is critical to identify subsets of the simulations and observations that represent
9 similar cloud/precipitation systems. To this end, a *TRMM Triple-sensor Three-step*
10 *Evaluation Framework* (T3EF) is introduced that systematically examines discrepancies
11 between the model and observations by i) creating joint diagrams of precipitating cloud
12 types from collocated VIRS Tb_{IR} and PR H_{ET} (Masunaga et al. 2005), ii) constructing
13 contoured frequency with altitude diagrams (CFADs) of PR reflectivity (Yuter and
14 Houze 1995) for each precipitating cloud type, and iii) constructing cumulative
15 probability distributions of TMI $PCTb_{85}$. Prior to actually evaluating the CRM, an
16 observational sketch of T3EF is introduced to address the physical aspects of each
17 radiance-based statistical evaluation.

18

19 **3.1 Joint Tb_{IR} - H_{ET} Diagrams**

20 Long-term simulations of the GCE model predict precipitating cloud ensembles
21 over the same periods as TRMM-observed tropical precipitation systems. Different
22 precipitating cloud systems are associated with different mesoscale processes and
23 therefore differing amounts of latent heat release, evaporative cooling, and radiative

1 heating (Tao et al. 2003; Olson et al. 2006). Consequently, it is critical to sub-categorize
2 and evaluate the frequencies of each of the different precipitating cloud systems
3 (Masunaga and Kummerow 2006). In this study, collocated VIRS Tb_{IR} and PR H_{ET} are
4 used to categorize tropical precipitation systems into shallow, cumulus congestus, deep
5 stratiform, and deep convective types closely following the methods in Masunaga et al.
6 (2005) (Figure 1). For the purpose of model evaluation, this method has an advantage
7 over traditional convective-stratiform separation methods (e.g., Lang et al. 2003) in that
8 identical radiance-based separation methods can be applied to both the TRMM
9 observations and simulator-coupled CRM simulations (Masunaga et al. 2008). It should
10 be noted that cumulus congestus overlapped by cirrus clouds can be erroneously
11 categorized into deep stratiform type in this scheme (Stephens and Wood 2007).

12 Figure 2 shows joint Tb_{IR} - H_{ET} diagrams from TRMM observations corresponding
13 to the SCSMEX and KWAJEX cases. In the KWAJEX case, the TRMM observations
14 show two distinct peaks in probability density ($\sim 1.2\% \text{ km}^{-1} \text{ }^\circ\text{K}^{-1}$): in the shallow category
15 with Tb_{IR} near 285°K and H_{ET} near 3 km and in the deep convective category with Tb_{IR}
16 near 210°K and H_{ET} near 8 km. In the SCSMEX case, the TRMM observations show a
17 strong peak in the deep convective category centered around 200°K (Tb_{IR}) and 10 km
18 (H_{ET}), higher probability densities in the deep convective category and less in the shallow
19 category. These results indicate that precipitation systems are much more organized and
20 vigorous in the SCSMEX case than they are in the KWAJEX case (Johnson et al. 2005;
21 Yuter et al. 2005; Zeng et al. 2007). In addition, the probability densities for the deep
22 stratiform type in the SCSMEX case appear to be smaller than those in the KWAJEX

1 case. Johnson et al. (2005) reported that the stratiform rain fraction (26%) for convective
2 systems from SCSMEX is smaller than that typical (40%) in the Tropics.

3

4 **3.2 Type-Classified Reflectivity CFADs**

5 CFADs are height-dependent probability density distributions of geophysical
6 parameters (Yuter and Houze 1995). Thus, CFADs of PR reflectivities provide a useful
7 statistical description that illustrates the effects of precipitation microphysics at different
8 altitudes (Lang et al. 2007; Zhou et al. 2007; Blossey et al. 2007). Lumping the different
9 precipitating cloud categories together in the analysis could, however, smear together the
10 important microphysical characteristics associated with each precipitating cloud type
11 (Lang et al. 2007; Blossey et al. 2007). For example, in the previous section, it was
12 shown that SCSMEX has a higher probability of deep convective clouds. As such,
13 grouping all of the cloud categories together would generate CFADs biased toward the
14 characteristics of deep convective clouds. In order to avoid this kind of bias, reflectivity
15 CFADs should be separately constructed for at least the convective and stratiform
16 portions of precipitation systems (Yuter et al. 2005; Zhou et al. 2007). This study
17 differentiates the CFADs into separate shallow, cumulus congestus, deep stratiform, and
18 deep convective categories as defined by the joint Tb_{IR} - H_{ET} diagrams.

19 Figure 3 shows type-classified reflectivity CFADs for the KWAJEX and
20 SCSMEX cases. Reflectivity CFADs were constructed by binning the reflectivities into
21 1-dBZ bins at each height increment (250m). Shallow is the weakest category in terms of
22 reflectivity intensity. Peak modal and maximum reflectivities are limited below 25 dBZ
23 and 44 dBZ, respectively. Cumulus congestus is a more vigorous category with larger

1 peak modal and maximum reflectivities than the shallow type. For shallow and cumulus
2 congestus types, the reflectivity distribution broadens towards the surface, indicating the
3 importance of coalescence and collection processes, which widen the raindrop spectra.
4 CFADs for the deep stratiform type appear to be relatively similar to those for cumulus
5 congestus, but the effect of melting ice particles is noticeable, especially in the SCSMEX
6 case along the edge of the CFAD (at an altitude of about 5km). The SCSMEX
7 precipitation systems likely produced larger ice particles aloft and consequently more
8 enhanced “bright bands” in the stratiform regions compared to those in KWAJEX.
9 Below the melting layer, the reflectivity distributions are relatively uniform with height
10 in contrast to the shallow and cumulus congestus types wherein the peak modes gradually
11 increased towards the surface.

12 The most remarkable CFADs are associated with the deep convective type. At
13 high altitudes (i.e., above 10km), reflectivities are narrowly distributed, and maximum
14 values remain below ~30 dBZ. These low PR reflectivities can be attributed to the
15 presence of smaller frozen precipitation particles. At middle altitudes (i.e., between 5
16 and 10 km), maximum reflectivities increase toward lower altitudes, which suggests a
17 broadening and increase in particle sizes due to the aggregation of frozen particles. Peak
18 modal reflectivity increases dramatically below 6 km due to the melting of frozen
19 particles. At low altitudes (i.e., below 5 km), frozen condensates are almost completely
20 melted, allowing liquid raindrops to dominate the radar backscattering signals. The high
21 dielectric constant of liquid water results in larger reflectivities than at high altitudes.
22 Reflectivity distributions below the melting layer are relatively uniform with height, an
23 indication that raindrop breakup and stochastic collection are combining to stabilize the

1 raindrop size spectra. Compared to KWAJEX, the SCSMEX deep convective category
2 has broader and larger reflectivities.

3

4

5 **3.3 Type-Classified Cumulative Probability Distributions of $PCTb_{85}$**

6 Although a passive microwave radiometer provides less specific information on
7 the vertical profiles of condensates than the TRMM PR, the 85-GHz TMI channels are
8 fairly sensitive to ice water path in the upper portions of precipitating cloud systems
9 (Yuter et al. 2005). At this frequency, precipitation-sized particles scatter the upwelling
10 microwave radiation emission, and thereby depress the outgoing microwave radiances at
11 the TOA (Liu and Curry 1996). Therefore, to augment the reflectivity CFADs, Tbs from
12 the TRMM satellite are assessed in terms of cumulative probability distributions of
13 $PCTb_{85}$ for the different precipitating cloud types. This evaluation is also important for
14 the assessment of passive microwave sensor-based rainfall/latent heating retrieval
15 algorithms, because the GCE simulations and simulated Tbs are used in the *a priori*
16 databases of retrieval algorithms (Kummerow et al. 2006; Olson et al. 2006).

17 Figure 4 shows cumulative probability distributions of $PCTb_{85}$ (bin size is 10°K).
18 It is quite discernible, particularly for the SCSMEX case, that the probability distributions
19 trend toward lower $PCTb_{85}$ values as the cloud types progress from shallow to cumulus
20 congestus to deep stratiform to deep convective. This essentially means that the amount
21 of frozen precipitation particles increases from shallow to deep convective type clouds. It
22 is worth noting that the probability distributions for the deep stratiform type have larger
23 $PCTb_{85}$ depressions than do the cumulus congestus type, although the structures of their

1 reflectivity CFADs appeared to be quite similar (Figure 3). This is a manifestation of
2 $PCTb_{85}$ depressions being highly sensitive to smaller-sized frozen precipitation particles,
3 to which the PR is relatively insensitive due to its longer wavelength. In contrast to
4 SCSMEX, the probability distributions for deep convective and deep stratiform types are
5 nearly the same in KWAJEX, although the CFADs for these two types are dissimilar
6 (Figure 3). The KWAJEX $PCTb_{85}$ depressions are also suppressed compared to those
7 from SCSMEX, an indication that deep convective precipitation is more isolated and less
8 vigorous in KWAJEX. These results highlight the utility of evaluating $PCTb_{85}$ in
9 addition to PR reflectivity.

10

11

12 **4. Evaluating the GCE simulations through T3EF**

13 This section, T3EF is used to evaluate the GCE simulations for KWAJEX and
14 SCSMEX. It should again be noted that TRMM-consistent radiances are computed from
15 the GCE simulations using multi-frequency satellite simulators, and those radiances are
16 then contrasted against observed radiances in a three-step statistical evaluation.

17

18 **4.1 Evaluation of Precipitating Cloud Types by Joint $Tb_{IR}-H_{ET}$ Diagrams**

19 Joint $Tb_{IR}-H_{ET}$ diagrams are constructed from the GCE simulations for two
20 different microphysics schemes (GM03 and GM07) using the satellite simulators (Figure
21 5). In the KWAJEX case, it is clear that both of the GCE experiments (i.e., GM03 and
22 GM07) strongly overestimate the probability densities of shallow and cumulus congestus
23 types; the combined shallow and cumulus congestus probability densities are 71.7% for

1 GM03 and 69.3% for GM07 compared with just 33.1% from the TRMM observations.
2 On the other hand, combined probability densities of the deep convective and stratiform
3 types (25.8% in GM03 and 28.8% in GM07) largely underestimate the TRMM
4 observations (65.2%). GM07 performs slightly better in terms of the Tb_{IR} (\approx cloud-top
5 temperature) probability distributions for deep stratiform and convective systems
6 compared to GM03. It should be noted that the probability densities for deep convective
7 clouds in the GCE simulations have a corrugated texture along the H_{ET} axis. This is an
8 artifact of the current GCE (and almost all other CRM) grid configurations that use a
9 stretched vertical coordinate, which results in a coarser layer thickness (~ 1 km) than the
10 PR resolution (0.25 km) in the upper troposphere.

11 Overall, the GCE performs better in the SCSMEX environment than in the
12 KWAJEX environment. The structure of the probability densities, particularly in GM03,
13 is similar to that of the TRMM observations. Although the combined deep convective
14 and stratiform precipitation probability densities (71.5% for GM03 and 82.2% for GM07)
15 slightly overestimate the TRMM observations (65.2%), the probability densities of
16 shallow precipitation are very close (9.01~11.5%). Unlike the KWAJEX case, GM03
17 performs slightly better than GM07. As noted earlier, there is a significant difference
18 between the KWAJEX and SCSMEX cases that is attributable to differences in the
19 environmental forcing and hence dynamics of the precipitation systems. The fact that the
20 GCE performs better for SCSMEX is probably due to it having more organized
21 precipitation systems driven by stronger large-scale forcing (Johnson et al. 2005), which
22 are better resolved by the 1-km horizontal grid spacing. The less vigorous KWAJEX

1 case probably requires a finer horizontal resolution to resolve the evolution of weaker,
2 isolated, less-organized cumulus systems as demonstrated by Lang et al. (2007).

3

4 **4.2 Evaluating Precipitation Microphysics by Type-Classified Reflectivity CFADs**

5 Instead of showing the entire probability distributions, the mean and maximum
6 reflectivities are highlighted and compared between the TRMM observations and GCE
7 simulations for the KWAJEX and SCSMEX cases. Although not shown here, the
8 minimum reflectivity is always 17 dBZ (the minimum PR-detectable echo) for all cases
9 (Figure 6).

10 *Shallow:* In both SCSMEX and KWAJEX, the mean reflectivity profiles of the
11 TRMM observations gradually increase from 18 dBZ at the echo top altitude to 25 dBZ
12 near the surface; both the GM03 and GM07 profiles from the model agree quite well with
13 these observations (within an accuracy of 2 dBZ). The maximum TRMM-observed
14 reflectivities in KWAJEX are slightly smaller (24 dBZ to 38 dBZ) than those in
15 SCSMEX (27 dBZ to 42 dBZ) but again, both are well captured by GM03 and GM07.

16 *Cumulus congestus:* Mean reflectivity profiles from the TRMM observations for
17 both cases range from 18 dBZ at the echo top altitude to 29 dBZ near the surface. While
18 the GCE simulations slightly overestimate the TRMM mean reflectivities by about 3
19 dBZ, the most discernible discrepancy between the model and observations appears in the
20 maximum reflectivity profiles for the KWAJEX case. The GCE simulations overestimate
21 the maximum reflectivities by as much as 16 dBZ near the echo top and by 10 dBZ near
22 the surface. The overestimated reflectivity in the upper layer is most likely due to the
23 presence of large frozen precipitation particles (see details in next section). For a given

1 drop-size distribution and number concentration, a 16-dBZ bias is equivalent to a mean
2 particle diameter in the GCE simulations that is nearly twice as large as that of the
3 TRMM observations in the Rayleigh approximation. As parameterized in the GCE, the
4 presence of large-sized particles will enhance the mean particle terminal velocity that
5 suppress deeper ice particle aloft. Thus, the presence of large ice-phase condensates could
6 explain why the GCE overestimates the frequency of cumulus congestus, while
7 underestimating the frequency of the deep convective and stratiform categories. On the
8 other hand, maximum reflectivities from the GCE simulations agree reasonably well with
9 the TRMM observations for the SCSMEX case. Model deviations from the observed
10 mean and maximum reflectivities are limited to 3 and 4 dBZ, respectively. In all cases,
11 there is almost no difference in performance between GM03 and GM07.

12 *Deep Stratiform:* Although the GCE simulations in this study do not produce a
13 robust melting signature in the reflectivity profiles, GM03 and GM07 generally agree
14 well with the TRMM observations in terms of the mean and maximum reflectivities
15 particularly in the KWAJEX case. In the SCSMEX case, GM03 and GM07 tend to
16 overestimate the maximum reflectivities by around 6 dBZ below an altitude of 4 km.
17 Below an altitude of 1 km, the TRMM observations show a strong reduction in the
18 maximum reflectivities probably due to rain evaporation. None of the GCE simulations
19 capture this feature. This is the most prominent difference between the modeled and
20 observed radar profiles for the deep stratiform type. Again GM03 and GM07 do not have
21 discernible differences in their reflectivity CFADs.

22 *Deep Convective:* Among the four different cloud types, the largest discrepancies
23 between the model and observations appear in the deep convective type. Although

1 GM07 does perform somewhat better at higher altitudes in the KWAJEX case, the GCE
2 simulations still generally do not capture the dramatic transitions in the reflectivity
3 profiles observed by the TRMM satellite. At high altitudes, GM03 overestimates the
4 mean and maximum reflectivities by as much as 5 dBZ and 12 dBZ, respectively, which
5 suggests that the GCE-simulated frozen precipitation particles are excessive both in size
6 and amount. Near the melting layer (~5 km), both GM03 and GM07 underestimate the
7 mean and maximum reflectivities by as much as 6 dBZ due to the lack of a melting
8 signature in the simulations. Near the surface, both GM03 and GM07 agree well with the
9 TRMM SCSMEX observations, but they tend to overestimate reflectivities for the
10 KWAJEX case. As discussed in other previous modeling studies (Zhou et al. 2007;
11 Blossey et al. 2007), the classified reflectivity CFADs highlight the uncertainties in the
12 microphysics of simulated mixed-phase clouds.

13

14 **4.3 Evaluating Ice Water Paths by Type-Classified Cumulative Probability**

15 **Distributions of $PCTb_{85}$**

16 Cumulative probability distributions of $PCTb_{85}$ were constructed from $PCTb_{85}$
17 values calculated from the GCE simulations for the KWAJEX and SCSMEX cases
18 (Figure 7). To better understand this statistical evaluation, condensates from the GCE
19 simulations are vertically integrated over the same sampling periods for the shallow,
20 cumulus congestus, deep stratiform, and deep convective types (Table 1).

21 *Shallow:* Due to the absence of appreciable amounts of ice particles in this
22 category (Table 1), cumulative probability distributions of shallow clouds can be
23 characterized by the following parameters: background Tb , radiance emission from

1 clouds, scattering of microwave radiance due to raindrops, and scattering of ice water
2 path from overlapped neighboring pixels. Errors in the background $PCTb_{85}$ are very
3 small, because the GCE simulations are forced by an observation-assimilated variational
4 analysis (Zhang et al. 2001). The emission of microwave radiance from cloud is also a
5 small contribution (Liu and Curry 1996). The amount of rain is also very small (Table 1).
6 Thus, discrepancies between the model and observations in the probability distributions
7 most likely represent noise from neighboring pixels. Because the conical-tracking view
8 of precipitation systems from the TMI channels is collocated with the cross-tracking view
9 from the VIRS and PR sensors, so is the combination of simulated radiances. In
10 particular, the GCE simulations for the SCSMEX case tend to have unrealistically large
11 depressions of $PCTb_{85}$ for the shallow type. Precipitation systems in SCSMEX are so
12 organized that shallow precipitation types are frequently accompanied with deep
13 convective precipitation. In addition, due to the cyclic boundary conditions used in the
14 GCE simulations, precipitation systems with fast propagation speeds tend to be densely
15 populated within the simulation domain. These factors increase the likelihood of deep
16 clouds overlapping shallow ones along the slant view of the TMI sensor.

17 *Cumulus congestus*: The GCE simulations tend to overestimate $PCTb_{85}$
18 depressions for both KWAJEX and SCSMEX. These depressions can also be attributed
19 to noise from neighboring pixels, but for cumulus congestus, the GCE simulates
20 appreciable amounts of snow and graupel that can increase $PCTb_{85}$ depressions (Table 1).
21 This is unlikely to be observed in real cumulus congestus as they commonly do not
22 glaciate (Johnson et al. 1999). The GM07 simulations produce less graupel than the
23 GM03, while increasing the combined amount of liquid cloud, rain, and snow (Table 1).

1 As graupel is defined to be a higher-density frozen particle in the GCE model and so too
2 in the passive microwave simulator, it has a greater single scattering albedo for a given
3 ice water content. As a result, the $PCTb_{85}$ depressions in GM03 are slightly reduced in
4 GM07. The GCE simulations for KWAJEX generate nearly twice as much graupel than
5 those for SCSMEX. This could explain the overestimation of maximum radar reflectivity
6 near echo top in the cumulus congestus for the KWAJEX simulations (Figure 6).

7 *Deep stratiform:* The GCE simulations slightly overestimate, but in general,
8 reasonably capture the observed probability distributions in the SCSMEX case. Probably
9 due to the relatively low amount of graupel (0.14 kg/m^2 , Table 1), the $PCTb_{85}$
10 depressions in GM07 are suppressed in comparison with GM03. In conjunction with the
11 reflectivity CFAD analysis, it appears that the GCE SCSMEX simulations fairly well
12 predict the precipitation-sized ice water path for deep stratiform systems in this particular
13 environment, which would lend more confidence to the passive-microwave retrieval
14 algorithms (Kummerow et al. 2006; Olson et al. 2006). Similarly, GM07 performs better
15 than GM03 for the KWAJEX case; however, both simulations overpredict $PCTb_{85}$
16 depressions, implying the GCE simulations contain too much precipitation-sized ice
17 (graupel and snow).

18 *Deep convective:* Similar to the deep stratiform type, the GCE overpredicts the
19 $PCTb_{85}$ depressions probably due to excessive amounts of frozen precipitation particles.
20 For both the KWAJEX and SCSMEX cases, GM07 performs better than GM03, because
21 GM07 tends to reduce the amount of high-density frozen condensate (graupel) in deep
22 convection by as much as $\sim 40\%$ (Table 1). These results suggest that simulated Tb_{85S}
23 from the GCE are biased toward lower values for deep convective precipitation.

1 Together with the reflectivity CFAD analysis (section 4.2), it appears that the GCE
2 generates too much frozen precipitation in deep convective clouds for both the KWAJEX
3 and SCSMEX cases. Note that large frozen particle amounts translate into larger particle
4 sizes in the exponential drop-size distributions with their fixed intercept. Therefore,
5 excessive amounts of simulated frozen particles could exacerbate the model biases in the
6 reflectivity CFADs and $PCTb_{85}$ probability distributions.

7

8 **5. Summary and Discussion**

9 Long-term simulations of convective cloud systems observed during SCSMEX
10 and KWAJEX using the GCE model are evaluated through via comparison between
11 TRMM observations and simulated radiances and reflectivities using multi-frequency
12 simulators in the Goddard SDSU. A proposed methodology for evaluating the simulated
13 radiances and reflectivities using three of TRMM's sensors, known as T3EF, was used to
14 systematically evaluate the performance of the GCE. While the GCE simulations are in
15 reasonable agreement with the TRMM measurements in some aspects, major simulation
16 biases found in this study include:

- 17 • A tendency for the GCE to overestimate the frequency of cumulus congestus and
18 underestimate the occurrence of deep convective and stratiform cloud types in
19 KWAJEX case.
- 20 • A tendency for the GCE to produce excessive amounts and therefore sizes of
21 frozen condensate in convective precipitation systems.

1 These biases appear to be common features in long-term CRM simulations with one-
2 moment bulk microphysics (Zeng et al. 2007; Zhou et al. 2007; Blossey et al. 2007), and
3 could be related to the following three issues:

4 i) *Large-scale forcing*: The long-term GCE simulations were driven by imposed
5 meteorological forcing obtained from variational analysis (Zhang et al. 2001).
6 This analysis blended all possible observations to obtain the best estimates of
7 area-averaged variables for the analysis domain over the KWAJEX and SCSMEX
8 sites. Unlike KWAJEX, the precipitation systems in SCSMEX are dominated by
9 mesoscale convective systems (MCSs) driven by stronger large-scale
10 environmental forcing (Johnson et al. 2005). Thus, it may be more realistic to
11 drive the GCE with area-averaged (~hundreds of kilometers) forcing from
12 SCSMEX than from KWAJEX .

13 ii) *Grid configurations*: In addition to the scale of the meteorological forcing, a finer
14 horizontal resolution in the GCE may be needed to better simulate the less-
15 organized precipitation systems in the KWAJEX case. For example, Lang et al.
16 (2007) found that GCE simulations using 1-km grid spacing tended to form deep
17 convection abruptly, while 250-m grid spacing realistically simulated the gradual
18 transition from shallow to deep convection that was observed during TRMM
19 Large-Scale Biosphere-Atmosphere Experiment in Amazonia (TRMM LBA).
20 However, at present, it is impractical to conduct long-term CRM simulations with
21 250-m grid spacing. This would require a lot more (~ 50 times) computing time.

22 iii) *Ice microphysics*: Besides the issues related to large-scale forcing and grid
23 configurations, the GCE simulates overly large radar reflectivities in the upper

1 troposphere and overly strong microwave *Tb* depressions. All of these results
2 suggest the bulk microphysics tends to simulate excessively large amounts and
3 sizes of precipitation ice. The new Goddard Microphysics (GM07) results in
4 some improvement in terms of microwave *Tbs* by reducing the amount of graupel;
5 however, it worsened the already poor estimation of shallow and cumulus
6 congestus frequencies in the SCSMEX case. The ice microphysics issues have
7 been discussed in previous modeling studies (e.g., Lang et al. 2007; Zeng et al.
8 2007; Zhou et al. 2007; Blossey et al. 2007). The overly large-sized precipitation
9 ice simulated by the model could enhance their terminal velocity and thus the
10 precipitation efficiency, suppressing deeper convection in the KWAJEX case.
11 This could be the reason that the GCE simulations generate too many cumulus
12 congestus and too few deep convective and stratiform systems in the KWAJEX
13 case. Blossey et al. (2007) proposed a similar hypothesis from their long-term
14 simulations for KWAJEX.

15 Technically, these three modeling deficiencies could interact nonlinearly, and complete
16 resolution of these deficiencies is not attempted in this manuscript. However, this paper
17 introduces a new practical CRM evaluation framework using direct satellite observations.
18 The new framework (T3EF), which uses multi-frequency satellite simulators and high-
19 resolution satellite radiance observations, revealed detailed errors in the CRM's
20 performance that could not be assessed by precipitation analysis only. Therefore, in
21 addition to the traditional comparisons between satellite products and simulations,
22 satellite simulator-based evaluation techniques will be most valuable for evaluating and
23 improving model performance. T3EF makes it possible to evaluate CRMs over most of

1 the Tropics, including over land and ocean. Therefore, with accurate large-scale
2 meteorological forcing, a satellite-radiance-based CRM inter-comparison study over
3 different tropical environments can be proposed in the near future.

4

5

6 **Acknowledgment**

7 This research was supported by the NASA Headquarters Atmospheric Dynamics and
8 Thermodynamics Program and the NASA Tropical Rainfall Measuring Mission
9 (TRMM). The authors are grateful to Dr. R. Kakar at NASA HQ for his support of this
10 research. This program was also supported by the NASA MAP. The authors are grateful
11 to Dr. D. Anderson at NASA HQ. The authors also acknowledge NASA GSFC and
12 Ames Research Center for computer time used in this research.

13

14

15

16

17

18

19

1 **References**

- 2 Blossey, P.N., C.S. Bretherton, J. Cetrone, and M. Kharoutdinov, 2007: Cloud-Resolving
3 Model Simulations of KWAJEX: Model Sensitivities and Comparisons with
4 Satellite and Radar Observations. *J. Atmos. Sci.*, **64**, 1488–1508.
- 5 Chaboureau, J.-P., J.-P. Cammas, P. J. Mascart, J.-P. Pinty, and J.-P. Lafore, 2002:
6 Mesoscale model cloud scheme assessment using satellite observations. *J.*
7 *Geophys. Res.*, 107(D16), 4301, doi:10.1029/2001JD000714.
- 8 Chevallier, F., and P. Bauer, 2003: Model Rain and Clouds over Oceans: Comparison
9 with SSM/I Observations. *Mon. Wea. Rev.*, **131**, 1240–1255.
- 10 Johnson, R.H., S.L. Aves, P.E. Ciesielski, and T.D. Keenan, 2005: Organization of
11 Oceanic Convection during the Onset of the 1998 East Asian Summer Monsoon.
12 *Mon. Wea. Rev.*, **133**, 131–148.
- 13 Johnson, R.H., T.M. Rickenbach, S.A. Rutledge, P.E. Ciesielski, and W.H. Schubert,
14 1999: Trimodal Characteristics of Tropical Convection. *J. Climate*, **12**, 2397–
15 2418.
- 16 Kidd, C., 1998: On rainfall retrieval using polarization-corrected temperatures. *Int. J.*
17 *Remote Sens.*, **19**, 981–996.
- 18 Kummerow, C., 1993: On the accuracy of the Eddington approximation for radiative
19 transfer in the microwave frequencies. *J. Geophys. Res.*, 98, 2757-2765.
- 20 Kummerow C., W. Barnes, J. Shiue, and J. Simpson, 1998: The Tropical Rainfall
21 Measuring Mission (TRMM) sensor package. *J. Atmos. Oceanic Technol.*, **15**,
22 809–817.

- 1 Kummerow, C., W. Berg, J. Thomas-Stahle, and H. Masunaga, 2006: Quantifying
2 Global Uncertainties in a Simple Microwave Rainfall Algorithm. *J. Atmos.*
3 *Oceanic Technol.*, **23**, 23–37.
- 4 Lang, S., W.-K. Tao, J. Simpson, and B. Ferrier, 2003: Modeling of convective-
5 stratiform precipitation processes: Sensitivity to partitioning methods. *J. Applied.*
6 *Meteor.*, 42, 505-527.
- 7 Lang, S., W.K. Tao, R. Cifelli, W. Olson, J. Halverson, S. Rutledge, and J. Simpson,
8 2007: Improving Simulations of Convective Systems from TRMM LBA:
9 Easterly and Westerly Regimes. *J. Atmos. Sci.*, **64**, 1141–1164.
- 10 Liu, G., and .A. Curry, 1996: Large-scale cloud features during January 1993 in the
11 North Atlantic Ocean as determined from SSM/I and SSM/T2 observations. *J.*
12 *Geophys. Res.*, **101**, 7019-7032.
- 13 Masunaga, H., T.S. L’Ecuyer, and C.D. Kummerow, 2005: Variability in the
14 Characteristics of Precipitation Systems in the Tropical Pacific. Part I: Spatial
15 Structure. *J. Climate*, **18**, 823–840.
- 16 Masunaga, H., and C.D. Kummerow, 2005: Combined Radar and Radiometer Analysis
17 of Precipitation Profiles for a Parametric Retrieval Algorithm. *J. Atmos. Oceanic*
18 *Technol.*, **22**, 909–929.
- 19 Masunaga, H., and C.D. Kummerow, 2006: Observations of Tropical Precipitating
20 Clouds Ranging from Shallow to Deep Convective Systems. *Geophys. Res. Lett.*,
21 **33**, L16805, doi:10.1029/2006GL026547
- 22 Masunaga, H., M. Satoh, and H. Miura, 2008: A joint satellite and global CRM analysis
23 of an MJO event: Model Diagnosis, *J. Geophys. Res.* (submitted).

- 1 Nakajima, T., and Tanaka, M., 1986: Matrix formulations for the transfer of solar
2 radiation in a plane-parallel scattering atmosphere. *J. Quant. Spec. Rad. Trans.*, 35,
3 13-21.
- 4 Olson W. S., and C. D. Kummerow, 1996: Simulated retrieval of precipitation profiles
5 from TRMM Microwave Imager and precipitation radar data. Preprints, *Eighth*
6 *Conf. on Satellite Meteorology and Oceanography*, Atlanta, GA, Amer. Meteor.
7 Soc., 248–251.
- 8 Olson, W.S., C.D. Kummerow, S. Yang, G.W. Petty, W.K. Tao, T.L. Bell, S.A. Braun,
9 Y. Wang, S.E. Lang, D.E. Johnson, and C. Chiu, 2006: Precipitation and Latent
10 Heating Distributions from Satellite Passive Microwave Radiometry. Part I:
11 Improved Method and Uncertainties. *J. Appl. Meteor. Climatol.*, **45**, 702–720.
- 12 Stamnes, K. H., S.-C. Tsay, W. Wiscombe, and K. Jayaweera, 1988: Numerical stable
13 algorithm for discrete-ordinate-method radiative transfer in multiple scattering
14 and emitting layered media. *Appl. Opt.*, **27**, 2502–2509.
- 15 Stephens, G. L., and N. B. Wood, 2007: Properties of tropical convection observed by
16 millimeter-wave radar systems, *Mon. Wea. Rev.*, **135**, 821–842.
- 17 Tao, W.K., 2003: Goddard Cumulus Ensemble (GCE) Model: Application for
18 Understanding Precipitation Processes. *Meteor. Monogr.*, **29**, 107.
- 19 Tao, W.-K., D. Starr, A. Hou, P. Newman, and Y. Sud, 2003: Summary of cumulus
20 parameterization workshop. *Bull. Amer. Meteor. Soc.*, 84, 1055-1062.
- 21 Tao, W.K., D. Anderson, R. Atlas, P. Houser, A. Hou, S. Lang, W. Lau, C. Peters-Lidard,
22 R. Kakar, S. Kumar, W. Lapenta, X. Li, T. Matsui, M. Rienecker, B.-W. Shen,

1 J.J. Shi, J. Simpson, X. Zeng, 2008: Goddard Multi-Scale Modeling Systems
2 with Unified Physics, GEWEX news letter, **18** (1), 6-9.

3 Yuter, S.E., and R.A. Houze, 1995: Three-Dimensional Kinematic and Microphysical
4 Evolution of Florida Cumulonimbus. Part II: Frequency Distributions of Vertical
5 Velocity, Reflectivity, and Differential Reflectivity. *Mon. Wea. Rev.*, **123**, 1941–
6 1963.

7 Yuter, S. E., R. A. Houze, Jr., E. A. Smith, T. T. Wilhelm, and E. Zipser, 2005: Physical
8 characterization of tropical oceanic convection observed in KWAJEX. *J. Appl.*
9 *Meteor.*, 44, 385-415.

10 Zeng, X., W.K. Tao, S. Lang, A. Y. Hou, M. Zhang, and J. Simpson, 2008: On the
11 sensitivity of atmospheric ensemble states to cloud microphysics in long-term
12 cloud-resolving model simulations, *Journal of the Meteorological Society of*
13 *Japan*, (In press).

14 Zhang, M. H., J. L. Lin, R. T. Cederwall, J. J. Yio, and S. C. Xie, 2001: Objective
15 analysis of the ARM IOP data: method and sensitivity. *Monthly Weather*
16 *Review*. 129, 295-311.

17 Zhou, Y.P., W.K. Tao, A.Y. Hou, W.S. Olson, C.L. Shie, K.M. Lau, M.D. Chou, X. Lin,
18 and M. Grecu, 2007: Use of High-Resolution Satellite Observations to Evaluate
19 Cloud and Precipitation Statistics from Cloud-Resolving Model Simulations. Part
20 I: South China Sea Monsoon Experiment. *J. Atmos. Sci.*, **64**, 4309–4329.

21
22
23

KWAJEX	Shallow		Cumulus Congestus		Deep Stratiform		Deep Convective	
	GM03	GM07	GM03	GM07	GM03	GM07	GM03	GM07
Cloud	0.16	0.16	0.35	0.37	0.03	0.27	0.24	0.31
Rain	0.12	0.12	0.70	0.78	0.18	0.46	1.39	1.33
Cloud ice	0.00	0.00	0.00	0.00	0.06	0.19	0.37	0.47
Snow	0.01	0.01	0.05	0.10	0.09	0.17	0.15	0.43
Graupel	0.01	0.00	0.31	0.23	0.24	0.19	2.32	1.42

SCSMEX	Shallow		Cumulus Congestus		Deep Stratiform		Deep Convective	
	GM03	GM07	GM03	GM07	GM03	GM07	GM03	GM07
Cloud	0.27	0.30	0.39	0.42	0.18	0.23	0.25	0.24
Rain	0.15	0.15	0.64	0.78	0.41	0.47	1.03	0.95
Cloud ice	0.00	0.00	0.00	0.00	0.07	0.28	0.65	0.88
Snow	0.01	0.01	0.04	0.08	0.12	0.25	0.22	0.82
Graupel	0.01	0.00	0.18	0.13	0.29	0.14	2.70	1.67

Table 1. Mean vertically-integrated condensates (kg/m^2) for shallow, cumulus congestus, deep stratiform, and deep convective types.

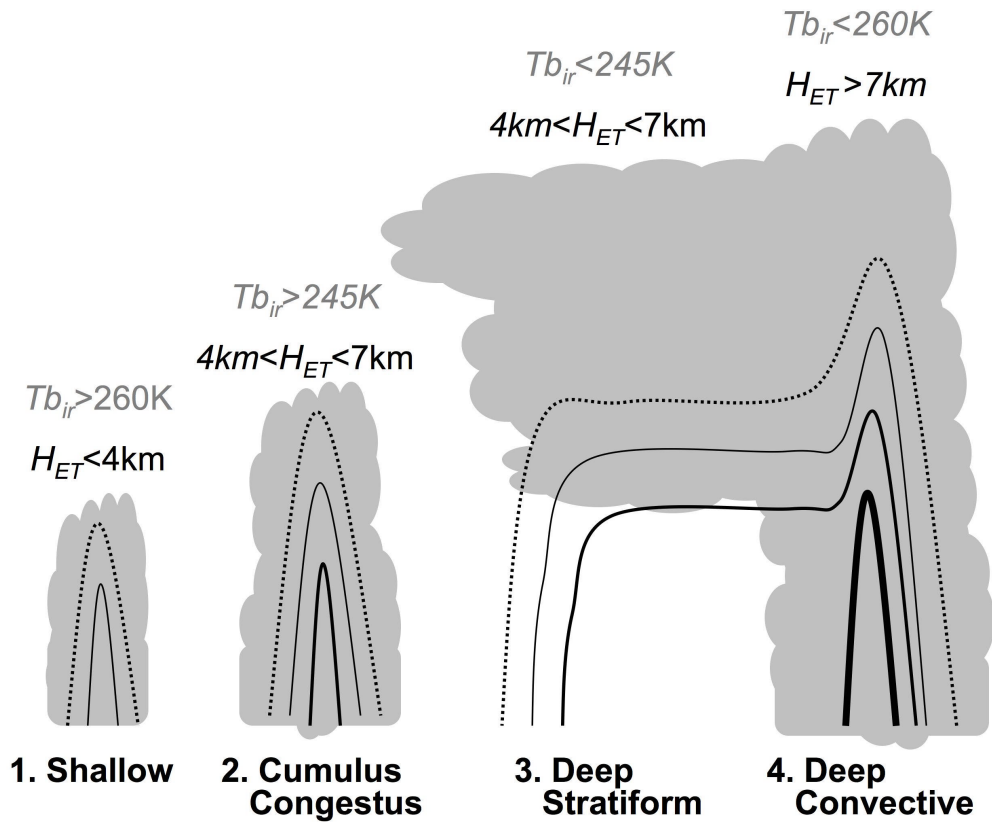


Figure 1. Schematics of precipitating cloud types closely following the method in Masunaga et al. (2005). Gray shading represents cloud ice and liquid condensates, and contoured lines represent precipitation radar reflectivity (dotted lines represent the minimum detectable radar echo while thicker solid lines represents larger echoes). Precipitation systems are categorized into 1) shallow, 2) cumulus congestus, 3) deep stratiform, and 4) deep convective systems based upon infrared brightness temperature (closely related to cloud-top temperature) and precipitation radar echo-top height (Masunaga et al. 2005).

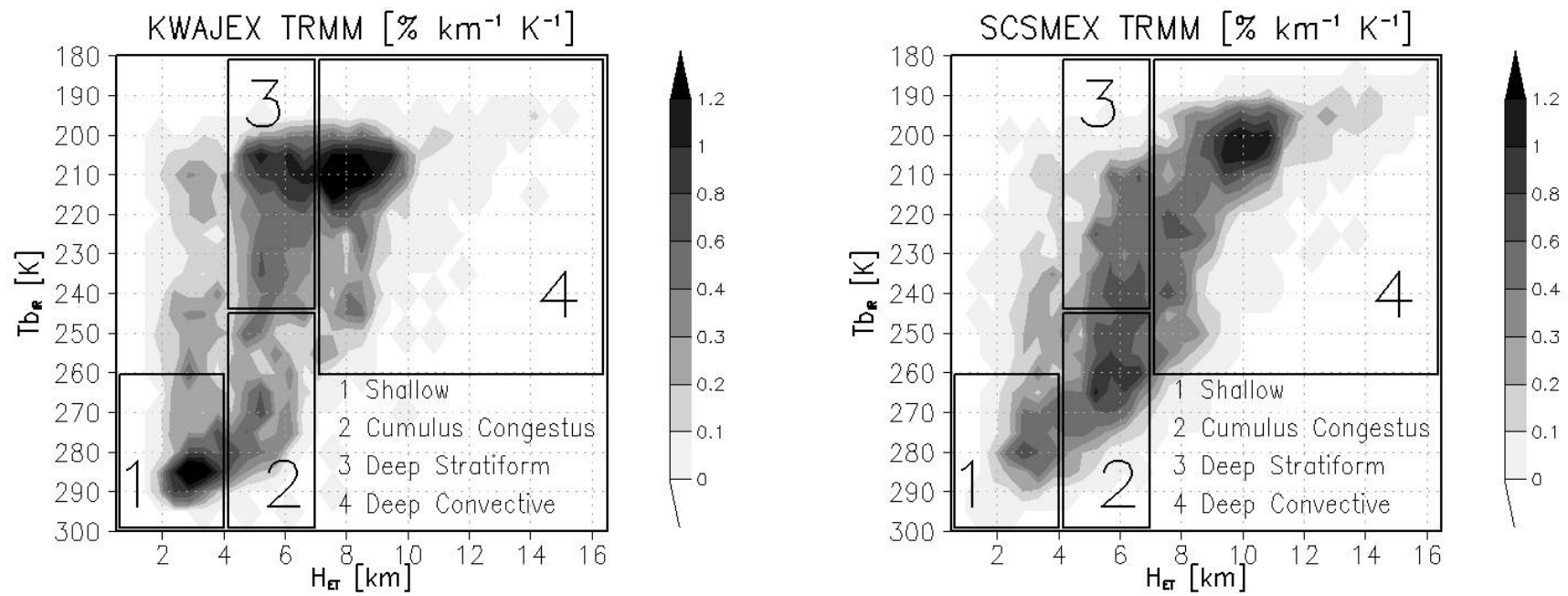


Figure 2. Joint infrared brightness temperature ($T_{b_{IR}}$)-radar echo-top height (H_{ET}) diagrams based on TRMM observations for the KWAJEX and SCSMEX cases.

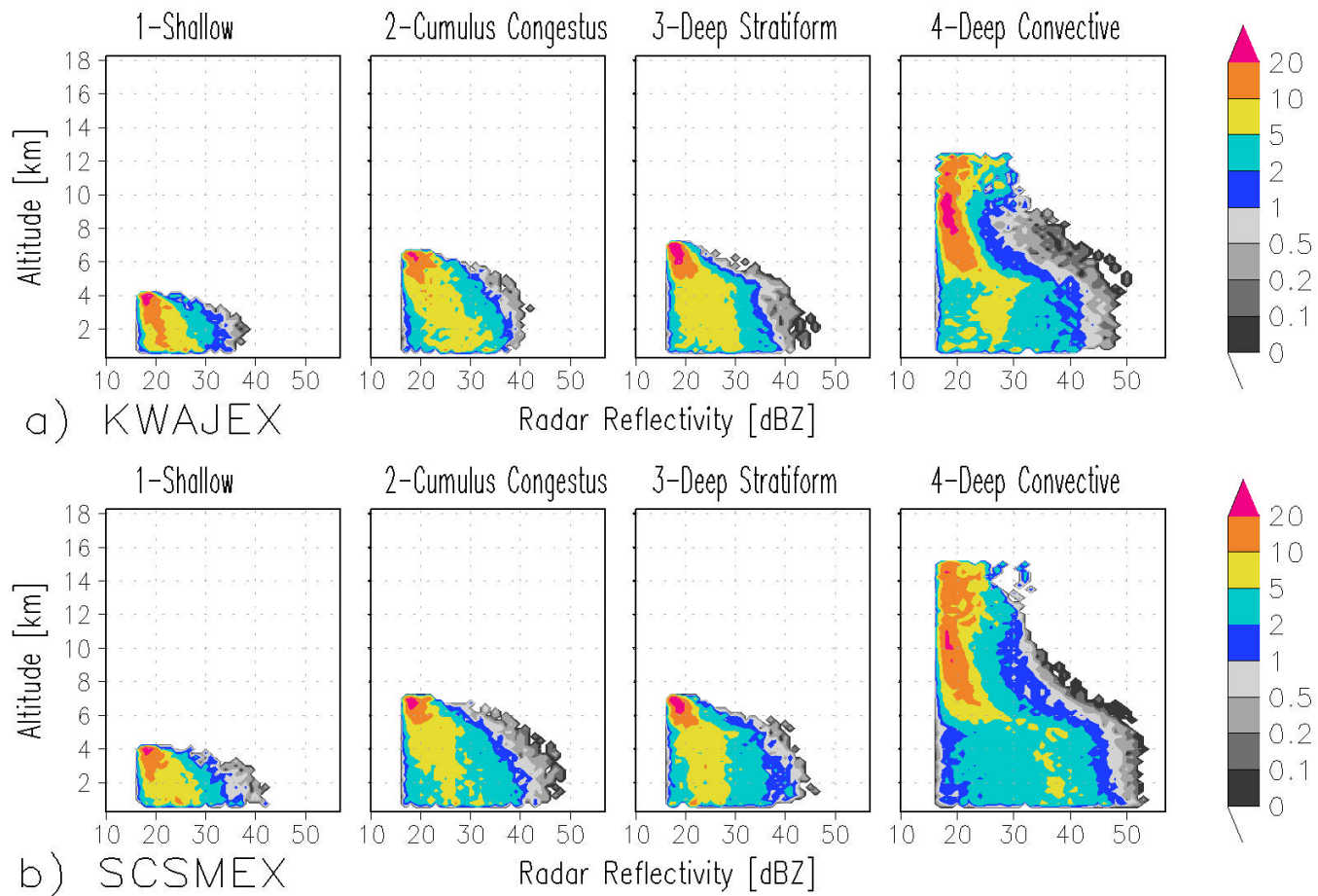


Figure 3. Contoured frequency with altitude diagrams (CFADs) of precipitation radar reflectivity for shallow, cumulus, deep stratiform, and deep convective types for a) KWAJEX and b) SCSMEX.

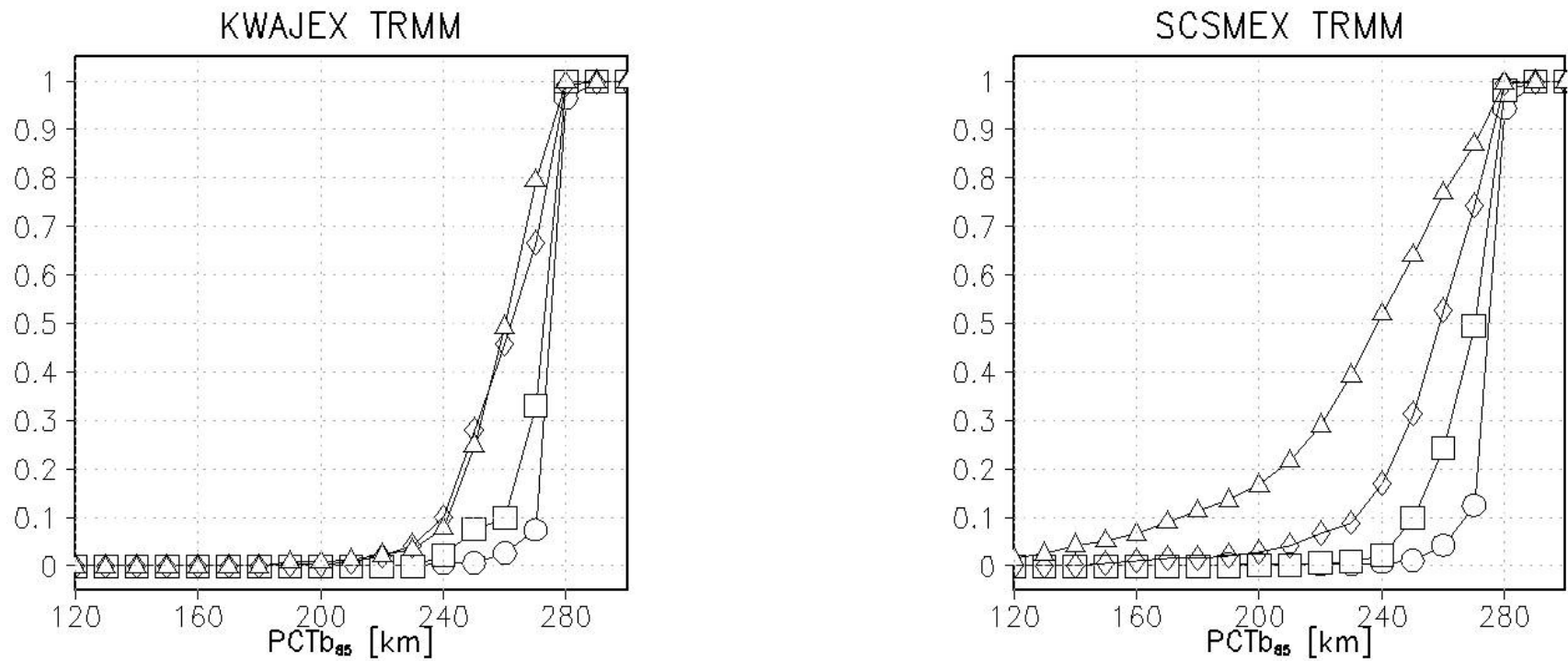
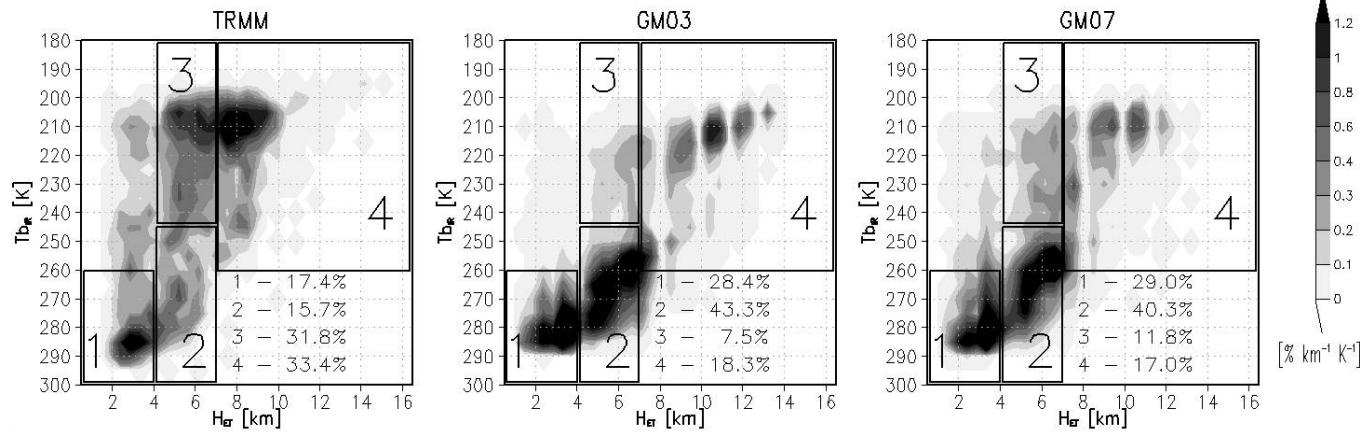
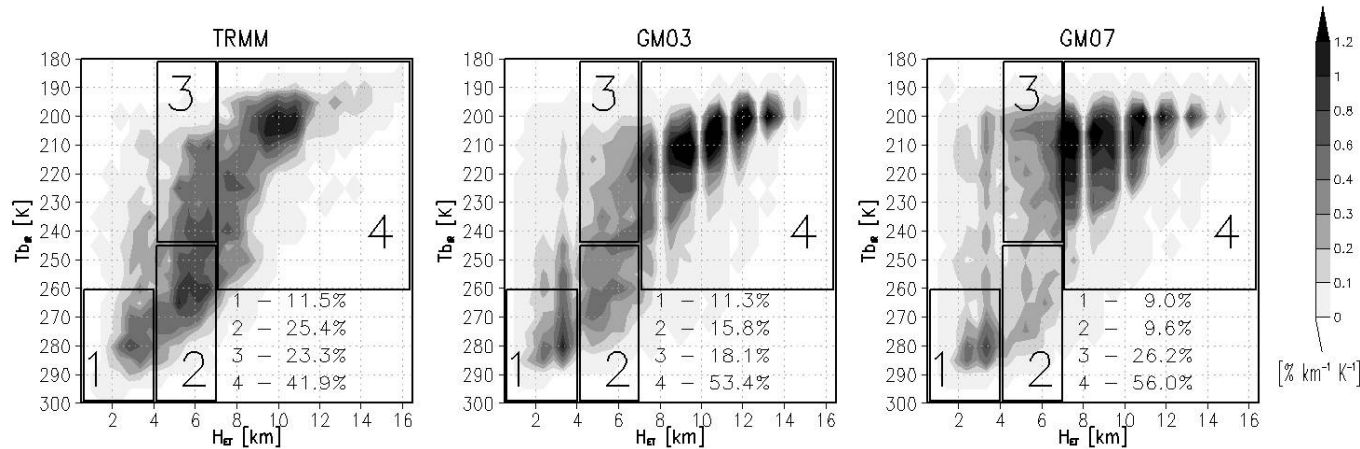


Figure 4. Cumulative probability distributions of polarization-corrected TMI brightness temperature at 85 GHz ($PCTb_{85}$: \circ shallow, \square cumulus congestus, \diamond deep stratiform, and \triangle deep convective) for KWAJEX and SCSMEX.



a) KWAJEX



b) SCSMEX

Figure 5. Comparison of joint Tb_{IR} - H_{ET} diagrams and probability densities for each precipitating cloud type between the TRMM observations and GCE simulations (GM03 and GM07) in a) KWAJEX and b) SCSMEX. Values represent the total probability densities for each (1-shallow, 2-cumulus congestus, 3-deep stratiform, 4-deep convective) precipitating cloud type.

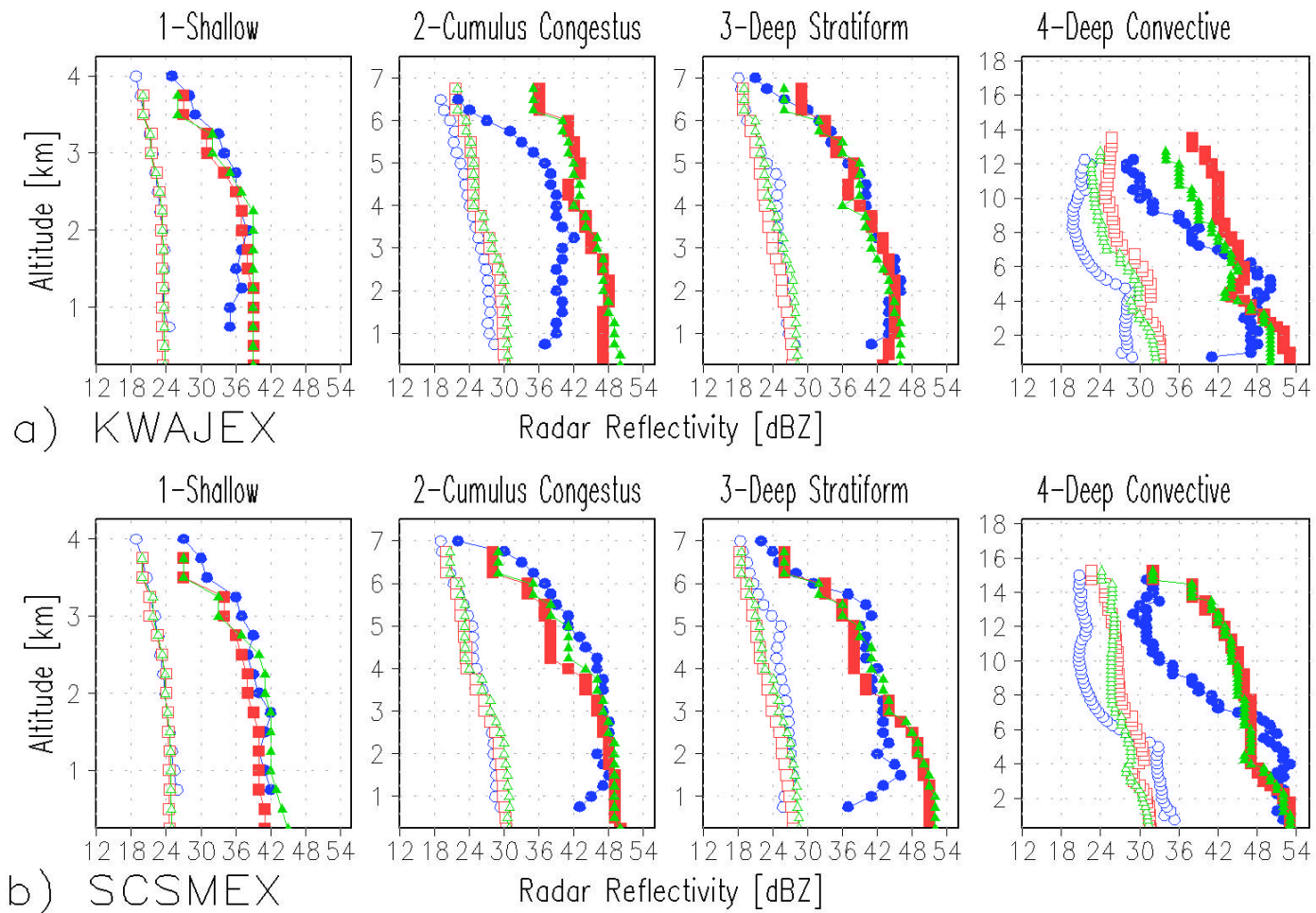
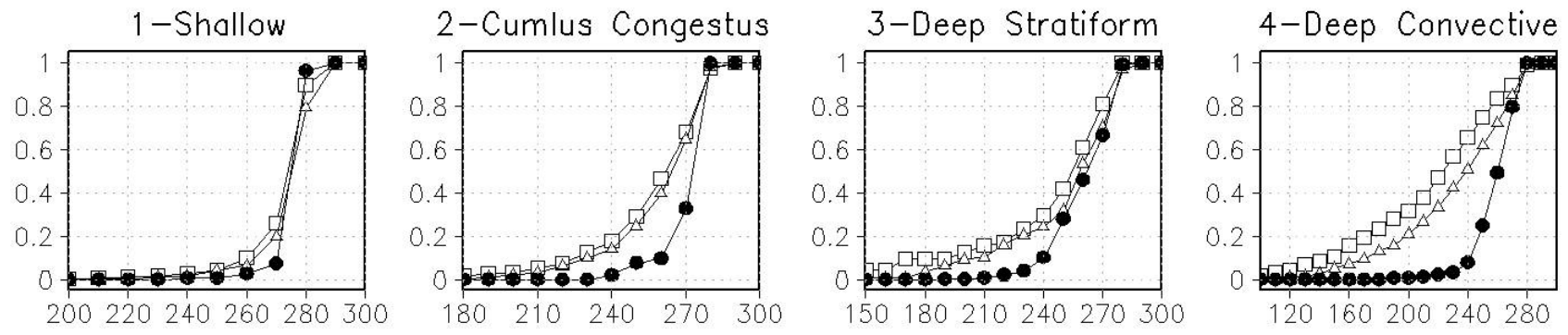
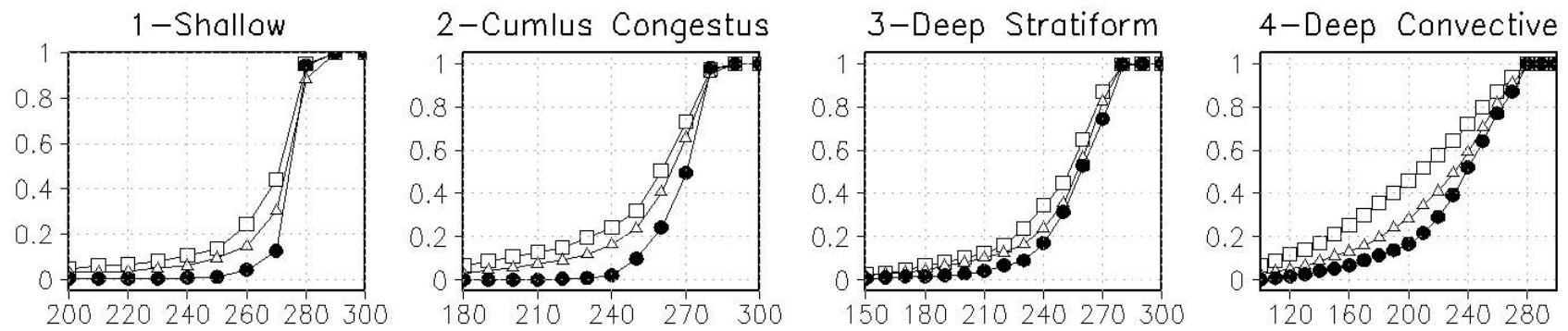


Figure 6. Mean (\circ TRMM, \square GM03, \triangle GM07) and maximum (\bullet TRMM, \blacksquare GM03, \blacktriangle GM07) reflectivity profiles from PR reflectivity CFADs for a) KWAJEX and b) SCSMEX cases. Different vertical scales are used for each type of precipitating cloud.



a) KWAJEX



b) SCSMEX

Figure 7. Cumulative probability distributions of polarization-corrected TMI brightness temperature at 85 GHz ($PCTb_{85}$: ● TRMM, □ GM03, △ GM07) for shallow, cumulus congestus, deep stratiform, and deep convective systems for a) KWAJEX and b) SCSMEX.